CCFE
CULHAM CENTRE FOR FUSION ENERGY

UK Atomic Energy Authority

UKAEA-CCFE-PR(23)178

J. Bland, J. Varje, N. Gorelenov, M. Gryaznevich, S.E. Sharapov, J. Wood

Interplay between beam-driven chirping modes and plasma confinement transitions in spherical tokamak ST40

Enquiries about copyright and reproduction should in the first instance be addressed to the UKAEA Publications Officer, Culham Science Centre, Building K1/0/83 Abingdon, Oxfordshire, OX14 3DB, UK. The United Kingdom Atomic Energy Authority is the copyright holder.

The contents of this document and all other UKAEA Preprints, Reports and Conference Papers are available to view online free at scientific-publications.ukaea.uk/

Interplay between beam-driven chirping modes and plasma confinement transitions in spherical tokamak ST40

J. Bland, J. Varje, N. Gorelenov, M. Gryaznevich, S.E. Sharapov, J. Wood

This is a preprint of a paper submitted for publication in Nuclear Fusion

Interplay between beam-driven chirping modes and plasma confinement transitions in spherical tokamak ST40

J. Bland[1], J. Varje[1], N.N. Gorelenkov[2], M.P. Gryaznevich[1], S.E. Sharapov[3], J. Wood[1] and the ST40 Team

[1]*Tokamak Energy Ltd, 173 Brook Drive, Milton Park, Oxfordshire OX14 4SD, UK*
[2]*PPPL, 100 Stellarator Rd, Princeton 08540, USA*
[3]*CCFE, Culham Science Centre, Abingdon, Oxfordshire OX14 3DB, UK*

This Letter reports on observed interplay between beam-driven modes of sweeping frequency (chirping modes) and transitions to the enhanced global confinement regime (H-mode) and back to the low confinement regime (L-mode) in the spherical tokamak ST40. The H-modes of plasma confinement are identified from decreased intensity of D_α signal and from clear distinctions in the edge gradients of the visible plasma boundary (observed as a sharp plasma edge in CCD images). The beam-driven chirping modes, identified as ideal MHD BAAE modes, are observed in Mirnov coil signals, interferometry, and soft X-ray diagnostics. A moderate amplitude "primer" chirping mode usually precedes an H-L transition. This is followed by a "dominant" chirping mode with higher amplitude during the L-mode. The L-H transition back to the improved confinement occurs on a longer time scale of tens of ms, consistent with the slowing down time scale of fast beam ions. A dramatic decrease in toroidal plasma rotation is systematically observed associated with chirping modes sweeping down to zero frequency. Resonance maps built for the beam-driven chirping modes with the ASCOT code show that the resonant beam ions have orbits near the trapped-passing boundary. The ASCOT modelling assesses how losses of the resonant fast ions caused by the chirping modes with high enough amplitude modify the torque, potentially affecting the plasma rotation.

PACs numbers: 52.55.Fa, 52.55.Pi, 52.35.Bj, 52.35.Py

The quality of plasma confinement is one of the key issues for designing and developing magnetic fusion machines [1]. The improvement of plasma confinement is one of the most important physics phenomena observed in magnetic fusion. It is essential to understand and to be able to predict confinement to design future next-step fusion tokamaks. Discovered in 1982 on the ASDEX tokamak [2], transitions from low plasma confinement (L-mode) to high confinement (H-mode) were found to occur when heating power of the plasma exceeds a certain threshold. This power threshold has a parametric dependence predominantly on the toroidal magnetic field, plasma density and plasma boundary surface area [3]. Theory developed for L-H transitions interprets this phenomenon as a result of a dynamical evolution of turbulence and transport in the main thermal plasma species based on the fundamental role of radial electric field E_r and plasma rotation shear suppressing the turbulence [4]. This Letter reports on a recent experimentally observed interplay between the beam driven core-localised modes of sweeping frequency (chirping modes) and quasi-periodic H-L-H transitions in the spherical tokamak ST40 [5]. These H-mode discharges had similar auxiliary heating power and plasma parameters in comparison to L-mode discharges, indicating their proximity to the ST40's power threshold in L-H transition. The observed interplay is somewhat similar to the high-frequency ELM precursors observed on PBX-M [6], but not on other magnetic fusion devices otherwise.

Figure 1 shows the observed correlation between the H-L-H transitions and chirping modes in a typical H-mode ST40 discharge (pulse #9823) with machine and plasma parameters: B_T = 2.1 T; I_P= 550 kA; a=0.27 m; R=0.5 m; κ=1.4, and NBI injected power of approximately 1 MW for the 55 keV NBI and 0.8 MW for the 25 keV NBI. Both the plasma and beam are deuterium. At the start of the time-range of interest (Figure 1) the plasma is in H-mode, as is seen from the low level of D_α signal in Figure

1c. At the onset of the chirping modes clearly visible in the magnetic signals (Figure 1a and 1b), transient H-L transitions are observed, with the intensity of D_α signal increasing by a factor of ~3. Then, the plasma transitions back into H-mode occurs with the D_α signal returning to the previous low levels. The whole H-L-H cycle looks like a transient phenomenon somewhat like ELMs but with a different characteristic time scale. When a sequence of the chirping modes occurs at ~125 ms, the H-L transition causes a longer L-mode dwell period rather than a transient H-L-H event. A zoom in the raw Mirnov coil signal is presented in Figure 2, which shows the build-up of small chirping (primer) modes of increasing amplitudes during the H-mode confinement period, followed by a larger (dominant) chirping mode that initiates during the fast H-L transition and continues into the L-mode period. This pattern of increasing amplitude primer modes followed by a single dominant mode can be observed for most (but not all) H-L transitions.

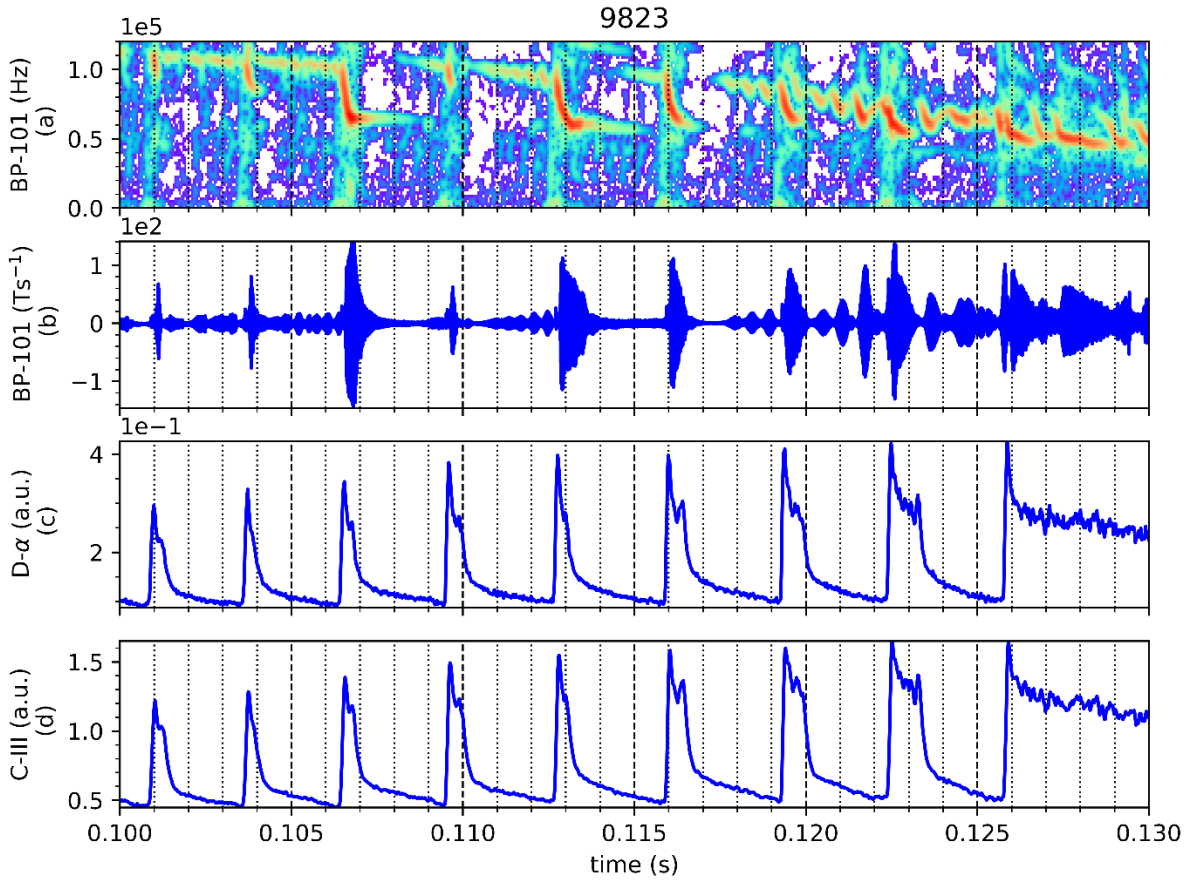

Figure 1. Top to bottom: (a) magnetic spectrogram from Mirnov coil showing amplitude (a.u.) and frequency pattern of the chirping modes; (b) raw Mirnov coil signal; (c) D_α signal; (d) C-III signal, with wavelength of 464.7 nm.

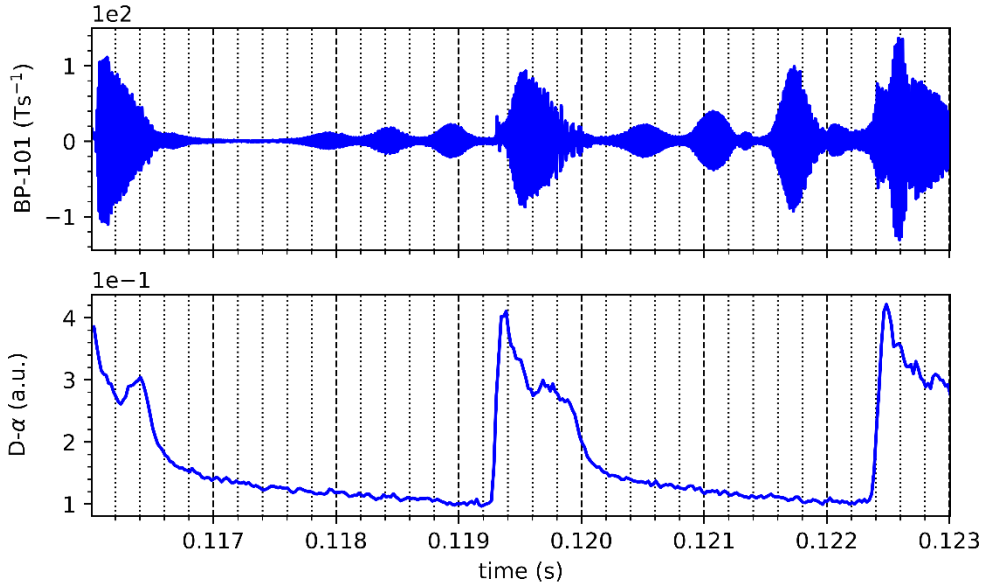

Figure 2. Zoom in for pulse 9823 of the raw Mirnov coil signal (top), and the D_α signal (bottom), illustrating the small chirping modes (primer) of increasing amplitude during the H-mode period, followed by the large amplitude (dominant) mode during the L-mode period.

Figure 3 shows that the spatial gradient of visible light emission changes notably in connection with the period of high D_α signal (Figure 1c 123 ms, Figure 3a) and low D_α signal (Figure 1c 125 ms, Figure 3b). The visible light seen in Figure 3b at low intensity has a much sharper boundary than the light in Figure 3a indicating a sharp plasma gradient in Figure 3b typical of the edge transport barrier in H-mode. The L-H transition power threshold, and further characterisation of H-mode observed in ST40 is discussed in [7]. Currently no edge profile diagnostics are available on ST40 to directly measure the presence of a pedestal.

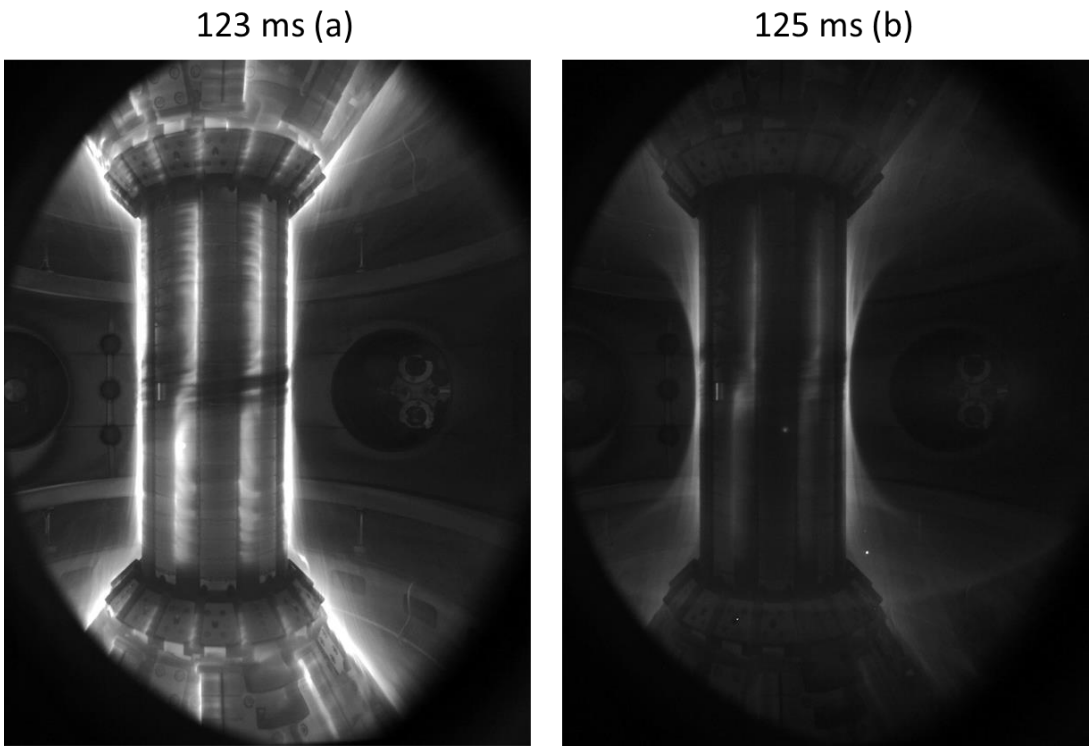

Figure 3. (a) Visible light image during L-mode at 123 ms; (b) visible light image observed during H-mode at 125 ms; Pulse 9823.

Chirping modes of the sub-TAE frequency range of ~70-100 kHz strongly correlates with the modulation of the D_α signal although some lower amplitude chirping modes in the much higher TAE frequency range of ~300-400 kHz also correlates in time with H-L transition at the early phase of the discharges. Chirping modes also seem to systematically correlate with decrease in toroidal plasma rotation in these series of discharges. The decrease in plasma rotation is best observed during the highest amplitude chirping modes, with the mode frequency going down to zero frequency, due to the limited temporal and intensity resolution of the plasma rotation diagnostic. Figure 4 shows three cases of this type when charge-exchange measurement detected a dramatic decrease of the plasma rotation during large amplitude chirping mode. The chirping mode itself transforms into a lock mode sweeping down to zero frequency in the end of its evolution. The toroidal plasma velocity is measured from the Doppler shift of line emission from charge-exchange process, C^{5+} (529nm). The measurement

uncertainty comes from the diagonal element of the covariance matrix of a least-square fit (one σ), taking known noise sources into account (ADC noise, Poisson noise from detected photoelectrons), but not systematic errors. Also present in Figure 4 is a lower amplitude mode around 50 kHz, which is also present in the BAAE gap according to calculations due to the broad gap width $\Delta\omega = (2\,v_A/R_0\,q)\delta\sqrt{1+2q^2}$ [8]. The subdominant mode is narrower and is located closer to the plasma centre with smaller gradient.

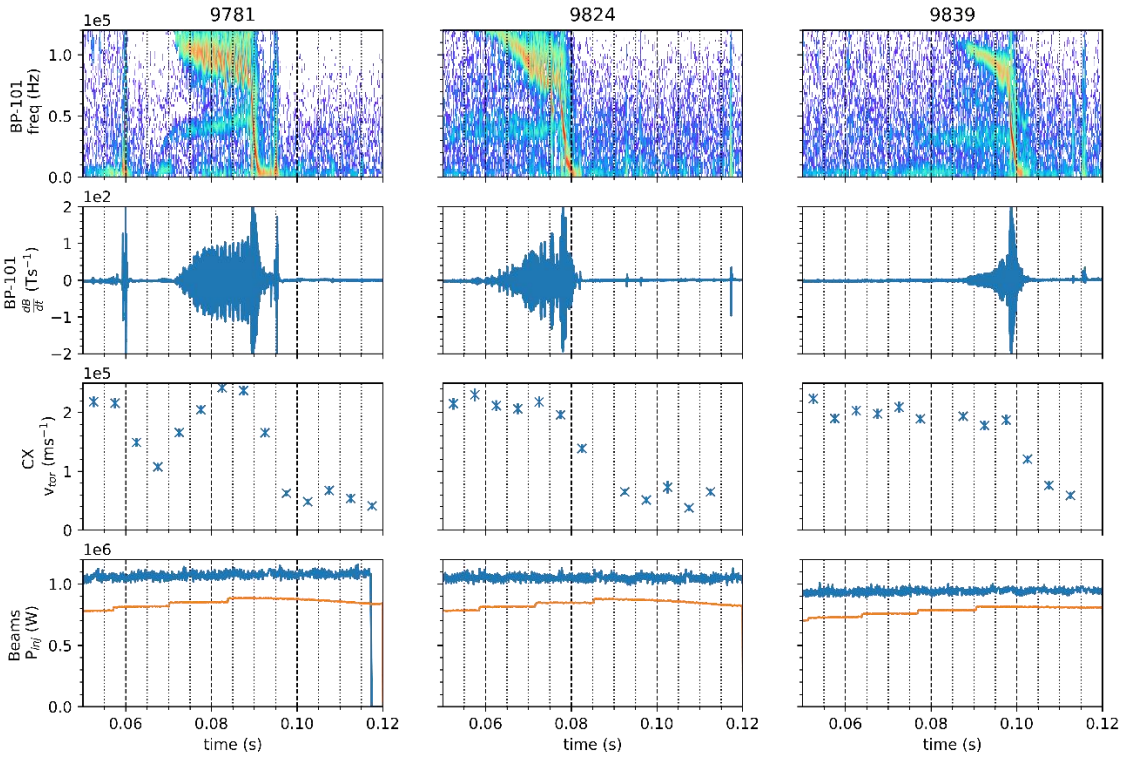

Figure 4. Top to bottom: magnetic spectrogram showing amplitude and frequency pattern of the chirping modes; raw Mirnov coil signal; toroidal plasma rotation measured at a major radius of 0.44 m with the line integrated charge-exchange diagnostic (r/a ~ 0.22); injected beam power of the two beams.

Figure 5 shows the presence of chirping modes in sub-millimetre (SMM) interferometer and SXR signals, in addition to the magnetic perturbation signal. The SXR system consists of 20 chords that form a fan in the vertical plane. As the presence of chirping modes is limited to chords that passed through the plasma centre, we conclude that the

chirping modes are localized deeply in the plasma core. Modelling performed with the NOVA code suggests these electromagnetic modes of sub-TAE frequency range are BAAE-modes [9], with radial mode structure similar to that obtained from the internal plasma measurements. For a fixed toroidal mode number n=1, the mode was comprised of a variety of poloidal harmonics, with m=1 having the largest amplitude.

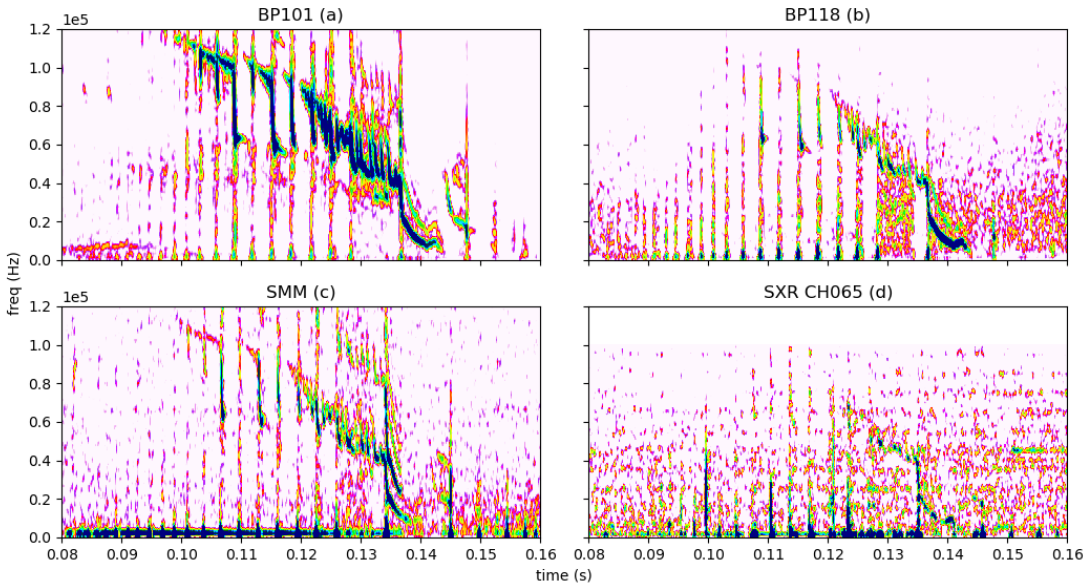

Figure 5. A set of chirping modes from pulse 9823 seen simultaneously in: (a) magnetic signal from an outboard Mirnov coil; (b) magnetic signal from an inboard Mirnov coil; (c) SMM interferometry signal; (d) SXR line-integrated signal for a single chord, orientated with an angle of ~0.45 degrees above midplane in the RZ plane (i.e. directed through the core of the plasma).

To assess the resonant beam-mode interaction and losses of energetic beam ions, the initial value particle-following ASCOT code [10] has been used. The simulations on the beam ion evolution were performed with an imposed core-localised n=1, m=1 MHD mode (Figure 6) as identified by simulations with the NOVA MHD spectral code [11], [12]. The resultant resonance maps between the beam drift orbits and a discrete frequency mode (f_{mode}) show how particle orbits of a given energy and pitch angle interact strongly with the specified mode in resonance. Figure 7a shows the overlaid

resonant maps for 70, 80 and 90 kHz mode frequencies, with a colour scale corresponding to the resonance condition expressed as $-\log(f_{mode} - n \times f_{b,tor} - p \times f_{b,pol})$, where $f_{b,tor}$ and $f_{b,pol}$ are the frequencies of the beam drift orbits in the toroidal and poloidal direction respectively, n is the toroidal mode number, and p is an integer. The high intensity resonance lines shown in Figure 7a have a very sharp gradient with respect to the pitch-angle but are almost constant as functions of the beam energy. The high energy resonance orbits circled in Figure 7a show the fast particle beam population that interacts with the mode. The types of the orbits resonating with the chirping modes are mostly those from the trapped-passing boundary (pitch angle $\frac{v_\parallel}{v} \lesssim v_{crit}$) as Figure 7b shows. The resonance preference of trapped particle orbits over passing orbits is due to the reduced poloidal and toroidal frequency of the trapped particle orbits, which lies closer to the mode frequency of interest. Note that the resonance curves go from the low energy thermal ions at $|v_\parallel/v| < 0.5$ to the high energy beam ions.

Figure 8a demonstrates the reduced fast particle content in the region $\rho < 0.2$ and corresponding reduction in the NBI torque. As the plasma's toroidal velocity prior to the mode is relatively fixed, the accelerating beam torque is matched by the opposing viscous torque, hence a reduction in beam torque would lead to a corresponding reduction in the plasma rotation, as observed in Figure 4. The reduction in toroidal plasma velocity by the modelled chirping modes could boost the turbulence and weaken the edge transport barrier of a H-mode plasma, leading to the plasma transitioning into L-mode. This provides a plausible explanation for the observed interplay between chirping modes and H-L-H mode transitions as observed in Figure 1. The pulse's proximity to the L-H power threshold also limits the size of perturbation needed, for the plasma to transition. Figure 8b divides the beam torque into its collisional and $J \times B$

components. This shows that the collisional torque is most strongly affected by the presence of the chirping mode, leading to the reduction in the net torque.

In Summary, this letter presents the experimental correlation between chirping modes and the plasma's transition from high to low confinement. Primer chirping modes are observed during the H-mode period, followed by a dominant chirping mode during L-mode. Further work is required to validate the preliminary theoretical explanations through additional fast particle simulations and integrated modelling simulations that incorporate beam torque to accurately determine its impact on plasma rotation, turbulence, and confinement.

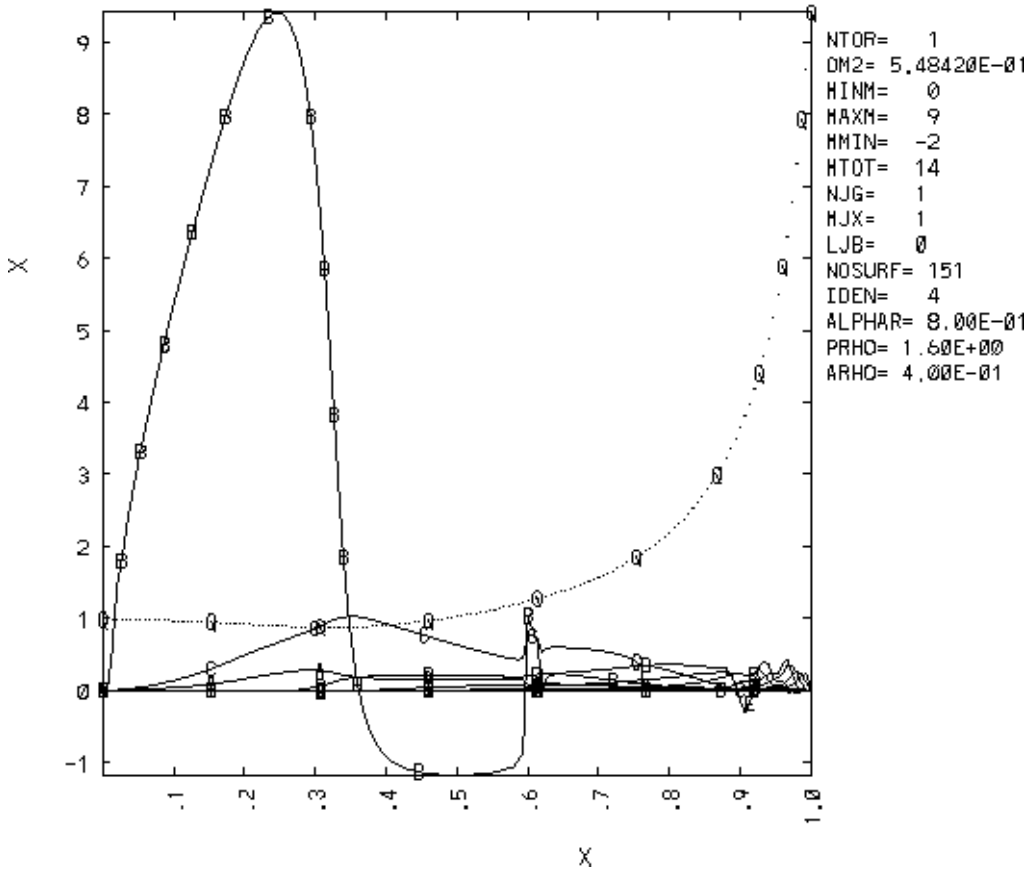

Figure 6. Radial profile of the BAAE mode for multiple poloidal harmonics observed during pulse 9781, at 8 ms. The dominant poloidal harmonic is m=1.

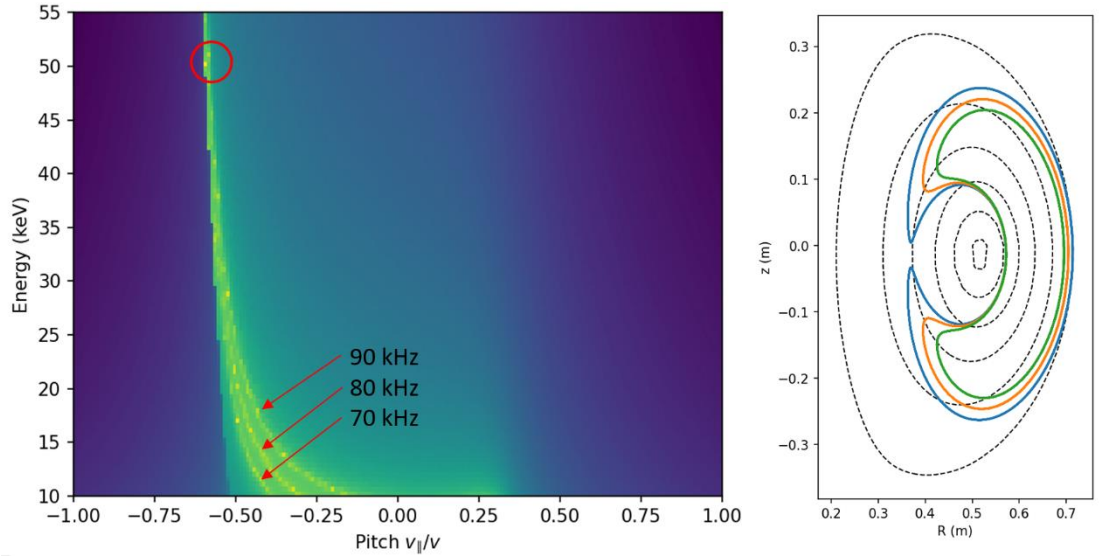

Figure 7. (a) Three resonance maps of the beam ions interacting with the chirping modes are shown for overlaid mode frequencies of 70, 80 and 90 kHz. The resonance condition is expressed as $-\log\left(f_{mode} - n \times f_{beam,tor} - p \times f_{beam,pol}\right)$. Pitch is defined as $v_\parallel/v$; (b) Drift orbits corresponding to the pitch-angles in (a).

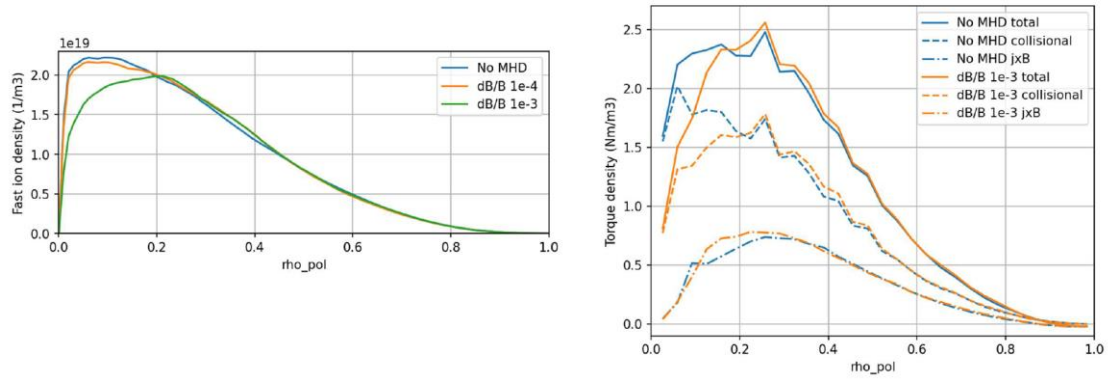

Figure 8. (a) How the MHD mode at 90 kHz with varying amplitudes impacts the radial profile of fast ion density. (b) Radial profile of the beam's torque density, split into collisional (momentum loss due to premature loss of fast ions) and $J \times B$ (particle drift or losses leading to a radial current that interacts with the poloidal B field) components, for both with and without the MHD mode.

Acknowledgements

We would like to thank Y. Andrew for useful discussions, in particular on H-mode confinement. The work of S.E.S. has been part-funded by the EPSRC Energy Programme [grant number EP/W006839/1].

References

[1] ITER Physics Expert Group on Energetic Particles, Heating and Current Drive and ITER Physics Basis Editors, "Chapter 5: Physics of energetic ions," *Nucl. Fusion*, vol. 39, no. 12, pp. 2471–2495, Dec. 1999, doi: 10.1088/0029-5515/39/12/305.

[2] F. Wagner *et al.*, "Regime of Improved Confinement and High Beta in Neutral-Beam-Heated Divertor Discharges of the ASDEX Tokamak," *Phys Rev Lett*, vol. 49, no. 19, pp. 1408–1412, Nov. 1982, doi: 10.1103/PhysRevLett.49.1408.

[3] Y. Andrew, J.-P. Bähner, R. Battle, and T. Jirman, "H-Mode Power Threshold Studies on MAST," *Plasma*, vol. 2, no. 3, pp. 328–338, Jul. 2019, doi: 10.3390/plasma2030024.

[4] F. Wagner, "A quarter-century of H-mode studies," *Plasma Phys. Control. Fusion*, vol. 49, no. 12B, pp. B1–B33, Dec. 2007, doi: 10.1088/0741-3335/49/12B/S01.

[5] M. P. Gryaznevich, "Experiments on ST40 at high magnetic field," *Nucl. Fusion*, Sep. 2021, doi: 10.1088/1741-4326/ac26ee.

[6] S. M. Kaye *et al.*, "Characteristics of high frequency ELM precursors and edge stability in the PBX-M tokamak," *Nucl. Fusion*, vol. 30, no. 12, pp. 2621–2627, Dec. 1990, doi: 10.1088/0029-5515/30/12/016.

[7] Y. Andrew *et al.*, "H-Mode Dithering Phase Studies on ST40," Philosophical Transactions A., submitted.

[8] N. N. Gorelenkov *et al.*, "Predictions and observations of global beta-induced Alfvén—acoustic modes in JET and NSTX," *Plasma Phys. Control. Fusion*, vol. 49, no. 12B, pp. B371–B383, Dec. 2007, doi: 10.1088/0741-3335/49/12B/S34.

[9] N. N. Gorelenkov, H. L. Berk, E. Fredrickson, S. E. Sharapov, and JET EFDA Contributors, "Predictions and observations of low-shear beta-induced shear Alfvén–acoustic eigenmodes in toroidal plasmas," *Phys. Lett. A*, vol. 370, no. 1, pp. 70–77, Oct. 2007, doi: 10.1016/j.physleta.2007.05.113.

[10] J. Varje *et al.*, "High-performance orbit-following code ASCOT5 for Monte Carlo simulations in fusion plasmas." arXiv, Aug. 07, 2019. Accessed: May 23, 2022. [Online]. Available: http://arxiv.org/abs/1908.02482

[11] C. Z. Cheng and M. S. Chance, "Low-n shear Alfvén spectra in axisymmetric toroidal plasmas," *Phys. Fluids*, vol. 29, no. 3695, p. 8, 1986.

[12] N. N. Gorelenkov *et al.*, "Beta-induced Alfvén-acoustic eigenmodes in National Spherical Torus Experiment and DIII-D driven by beam ions," *Phys. Plasmas*, vol. 16, no. 5, p. 056107, May 2009, doi: 10.1063/1.3097920.